Effect of pH on the electrochemical properties of polyaniline nanoparticle suspension in strongly acidic solution: an experimental and theoretical study

Fatemeh Biabangard, Hadiseh Nazari & Reza Arefinia

Journal of Solid State Electrochemistry
Current Research and Development in Science and Technology

ISSN 1432-8488

J Solid State Electrochem
DOI 10.1007/s10008-020-04863-0

Springer

Journal of Solid State Electrochemistry
https://doi.org/10.1007/s10008-020-04863-0

ORIGINAL PAPER

Effect of pH on the electrochemical properties of polyaniline nanoparticle suspension in strongly acidic solution: an experimental and theoretical study

Fatemeh Biabangard[1] · Hadiseh Nazari[1] · Reza Arefinia[1]

Received: 14 August 2020 / Revised: 8 October 2020 / Accepted: 6 November 2020

Abstract

A stable suspension of nanopolyaniline (nPANI) particles can be used in various applications instead of a polyaniline film. The electrochemical behavior of a stable suspension of nPANI particles, in strongly acidic conditions of HCl at the gold electrode surface, was investigated using various electrochemical and surface analysis methods. Voltammetry results showed two redox transformations indicating the adsorption and diffusion-controlled mechanism of nPANI particles. Moreover, the decrease in pH causes an increase in the number of electrons transferred per nPANI particles. The adsorption data were fitted by the Langmuir adsorption isotherm and the maximum surface coverage decreases with the increment of pH. The adsorption of nPANI particles was confirmed by the surface analysis methods. Moreover, the quantum chemical calculation and Monte Carlo simulation approved the electrochemical results for the effect of pH on the adsorption of nPANI particles at the gold electrode surface.

Keywords Nanopolyaniline particles · Redox behavior · Adsorption · Diffusion · Quantum chemical calculation

Introduction

Polyaniline (PANI) is the most famous conducting polymer from both the fundamental and application viewpoints due to its unique properties such as easy synthesis, different oxidation states, good redox reversibility, electrical and optical properties, and reasonable price [1–3]. The redox behavior of PANI provides the great attention in many applications such as medical [4, 5], electrochemical sensors [6, 7], supercapacitors [8–10], rechargeable batteries [11, 12], anti-corrosion agents [13–15], and ion exchange [16, 17].

Generally, PANI can be obtained in three main oxidation states: leucoemeraldine (LE), its completely reduced form; emeraldine (EB), its half oxidized form; and pernigraniline (PE), its completely oxidized state [18, 19]. The EB form is nonconductive in its nature but it can be converted to the conductive form, namely emeraldine salt (ES), by protonating in an acidic environment (doping process). The redox properties of PANI depend strongly on both its oxidation state and protonation level [20, 21]. On the other hand, many factors such as the potential range [20], solution pH [22–24], and temperature [25] affect the redox behavior of PANI.

From the practical viewpoint, solution pH in different applications has a great influence on the properties of PANI. As an example, a new type of ion exchangers works on the basis of the doping/de-doping processes of PANI, depending on the pH of the solution [26, 27]. In the case of PANI film, Scotto et al. [23, 28] studied the electrochemical behavior of a PANI film in various strongly acidic solutions and Ping et al. [29] reported the significant effect of solution pH in a wide range of variations on the redox behavior of PANI.

In these works, PANI film was applied on the electrode surface by the electrodeposition and drop-cast methods. However, from a practical point of view, these methods may have some problems such as the application on the electrodes with a large surface area. In order to overcome these problems, we suggested that using a stable suspension of polyaniline particles in nanoscale is an advantageous method [30, 31] where it showed the electrochemical behaviors like those observed for a PANI film. Therefore, this system may be a good candidate for the replacement of the PANI film which was

✉ Reza Arefinia
arefinia@um.ac.ir

[1] Chemical Engineering Department, Faculty of Engineering, Ferdowsi University of Mashhad, Mashhad, Iran

Published online: 16 November 2020

conventionally used in many applications. In this regard, the main redox behaviors of PANI suspension in strongly acidic conditions have not been investigated.

The aim of the present work is to study the effect of pH varying in the strongly acidic region (from − 0.6 to 1.0) on the electrochemical behavior of the suspension of nanopolyaniline (nPANI) particles at the gold electrode surface. The stability of suspensions prepared in hydrochloric acid was examined over time using UV–vis spectrum technique and zeta potential measurement. The electrochemical behavior of nPANI suspension at the gold electrode surface was studied by electrochemical methods of cyclic voltammetry (CV) and chronoamperometry. The accuracy of electrochemical data was examined using the surface analysis method of field emission scanning electron microscopy (FE-SEM) and the constituent elements adsorbed on the electrode surface were analyzed by the energy-dispersive X-ray spectroscopy (EDX) technique. Moreover, the adsorption process of nPANI particles, in the conditions similar to the experimental tests, was theoretically evaluated using the quantum chemical calculations and Monte Carlo (MC) simulations.

Experimental section

Preparation and characterization of suspensions

Nanopolyaniline (nPANI) particles were prepared according to the procedure that was in detail reported in previous work [32]. The nPANI suspensions were prepared upon ultrasonic dispersion of 100 ppm nPANI particles in a 3.7 M HCl solution (at pH − 0.60) for about 2 min. Furthermore, different pH values (− 0.60, − 0.20, 0.05, and 0.70) were adjusted by addition of NaOH solution, while the solution pH was simultaneously measured by using a pH meter (S230-USP/EP) equipped with a special glass electrode which is suitable for the acidic environment.

The stability of nPANI suspensions was evaluated with zeta potential measurement (Zeta Compact, CAD instruments, France) and Cary 50 UV–vis spectrophotometer.

Electrochemical experiments

All the electrochemical experiments were carried out by Autolab potentiostat/galvanostat model 302N at room temperature in a conventional electrochemical cell including the gold working electrode with an area of 1 cm^2, silver/silver chloride (Ag|AgCl) as a reference electrode and platinum wire as a counter electrode.

Before the electrochemical tests, the surface of the gold electrode was carefully treated according to the procedure that was reported in detail in previous work [30]. In addition, solved oxygen was removed from the system by bubbling highly purified nitrogen and then, a nitrogen purge was kept on the surface of suspension during the experiments.

The voltammetry tests were conducted with a potential sweep from − 200 to + 700 mV (vs. Ag/AgCl) for 10 cycles for different scan rates from low to high values (5 to 100 mV/s). It must be mentioned that after recording the CV diagrams, the background current was subtracted [30, 33] by insertion of an appropriate baseline [34].

Chronoamperometry tests were carried by applying an appropriate potential, selected with respect to the CV data, at different concentrations of nPANI particles, changed from 0 to 100 ppm. It is worth noting that the electrochemical tests were repeated several times to obtain very stable and reproducible data.

Surface analyses

After the chronoamperometry test, the surface of the electrode was studied using a field emission scanning electron microscope (FE-SEM, MIRA3 TESCAN) and the elemental analysis was performed by the energy-dispersive X-ray spectroscopy (EDX) technique.

Theoretical calculation methods

In the present study, all the calculations were performed using the Material Studio v 8.0 Accelrys Inc. software. The quantum chemical investigations were implemented with $DMol^3$ modulus based on the density functional theory (DFT). The molecular structures of PANI have been geometrically optimized using the m-GGA/M06-L level and DNP basis set. Fine convergence criteria and global orbital cutoff were used on the basis of set definitions. The Monte Carlo (MC) simulation was used to investigate the adsorption mechanism of polyaniline on the Au (110) plane surface via the adsorption locator module, COMPASS force field, and periodic boundary conditions.

Results and discussion

Characterization of nPANI-HCl suspension

The PANI particles had a spherical shape in nanoscale ranging between 20 and 50 nm according to previous works [32, 35]. The pH of HCl suspensions containing 100 ppm nPANI particles was changed in a range between − 0.2 and 0.7. These systems were placed under a stable condition without atmospheric exposure for 7 days. After this time, the suspension stability was investigated using a zeta potential analyzer where the zeta potential values were about 40 mV for both solution pH suggesting the electrostatically stability of suspensions [36].

Furthermore, the dispersion stability of nPANI particles within HCl solution at pH − 0.20 and 0.70 was evaluated by UV–vis spectroscopy for the times of 1 h and 7 days and is shown in Fig. 1. Regarding the y-scale of UV diagrams, it can be found that at both pH values, there is a negligible difference between the spectra recorded over 7 days, indicating the physically stability of suspensions and hence no important precipitation occurs at this span time, which is in agreement with the zeta potential data.

Moreover, Fig. 1 shows that at the polaron band at 700–740 nm, polaron–π* transition of the quinoid band at 430–450 nm and the π–π* transition of the benzenoid segment at 340–360 nm demonstrates the formation of ES structure of PANI particles [37, 38].

It is noticeable that the discrepancy of the spectral shapes in the wavelength range of 340–440 nm can be related to the difference in the intrachain conformation and doping effectiveness of the polymer backbone. In this regard, the absorbance ratio of benzenoid to the quinoid band and polaron (700–740 nm) to the benzenoid band can be considered as a measure of oxidation and doping levels of polyaniline, respectively [32].

Cyclic voltammetry measurements

The pH dependence of the redox properties of nPANI particle suspension in strongly acidic media was studied by cyclic voltammetry method and the CV curves for 100 ppm nPANI particles, dispersed in HCl solution at different pHs (− 0.60, − 0.20, 0.05, 0.70) are shown in Fig. 2. It is obvious that for all values of pH, the shape of CV curves is similar to each other. The first oxidation peak is related to the conversion of LE to the ES form of polyaniline [26], where the relevant reduction peak cannot be identified [39]. At the higher potentials, there exists another couple of oxidation-reduction peak corresponding to the transformation between ES and pernigraniline (PE) [40, 41]. These observations are similar to those addressed in the literature by other researchers [20, 42, 43]. Moreover, at pH = − 0.60, a pair of pre-peak can be identified in Fig. 2 which can be attributed to the adsorption behavior of nanoparticles in the electrode surface; however, it disappears at the higher values of pH [44].

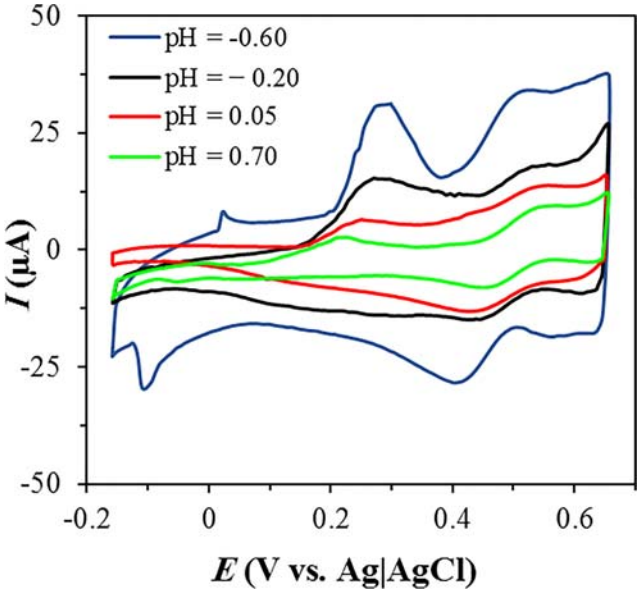

Fig. 2 Cyclic voltammograms of 100 ppm nPANI particles dispersed in HCl solution at different pHs. Scan rate: 30 mVs^{-1}

Variations of peak potential and peak current as a function of pH for two oxidation processes of nPANI-HCl suspension are shown in Fig. 3. In the case of the first oxidation peak (Fig. 3a), it is apparent that the increase of pH is generally associated with a shift of potential to the lower values due to the easier doping process (transformation of LE to ES) [20, 24, 45] and a reduction in the value of peak current (I_p) likely due to a decrement in the protonation degree of polyaniline structure as reported previously [20, 23].

Detailed inspection of Fig. 3a reveals that the trend of variation for peak potential (E_p) versus solution pH can be divided into two distinct regions. In the first region (between − 0.6 and 0.05), there is a linear relation between peak potential and pH with a slope of about 60 mV per pH unit. This finding, according to the Nernst equation, indicates that the number of

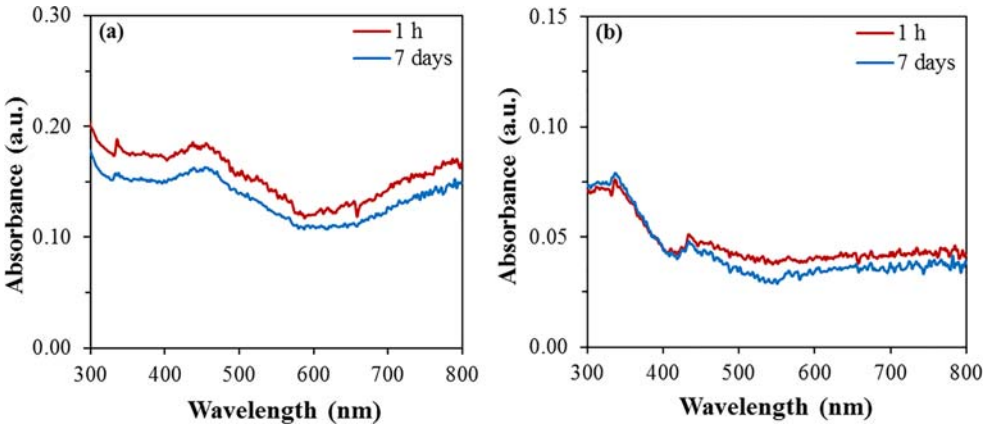

Fig. 1 UV–vis spectra of nPANI-HCl suspension at pH: a − 0.20 and b 0.70 after 1 h and 7 days

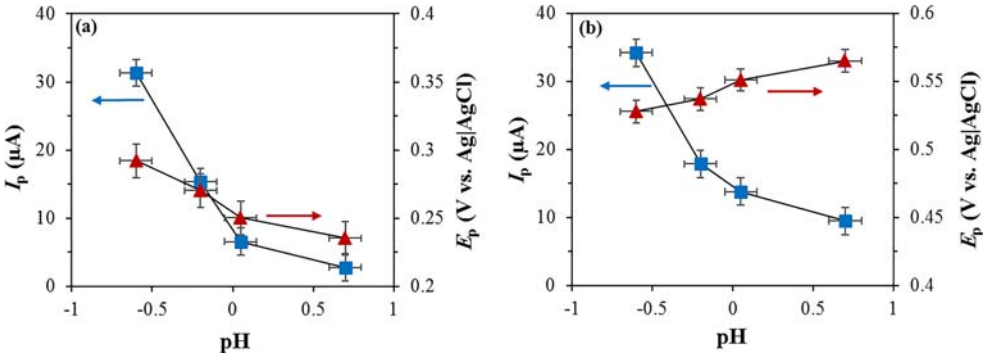

Fig. 3 The effect of pH on the peak current and peak potential of first (**a**) and second (**b**) oxidation steps of nPANI particle suspension in HCl solution. Scan rate: 30 mVs^{-1}

exchanged electron and proton is equal for the oxidation process as reported by MacDiarmid for a PANI film [20]. In other words, it can be stated that in this region, the protonation process of nPANI particles is performed, completely. For the second region (pH > 0.05), it seems that the effect of pH on the variation of E_p is significantly reduced suggesting that the protonation process occurs partly [23, 28, 46]. Moreover, Fig. 3a shows that the trend of variation of I_p is consistent with that observed for the variation of E_p.

For the second oxidation peak, Fig. 3b shows that an increase in pH from − 0.60 to 0.70 causes a decrease in the peak current probably due to the same reasons that discussed for the first oxidation peak; however, no significant change can be observed for the values of peak potential.

To determine, the controlling mechanism (diffusion or adsorption) of the electrochemical behavior of nPANI particles for each oxidation step, the cyclic voltammetry was conducted at different pHs (− 0.60, − 0.20, 0.05, 0.70) and various scan rates (from 5 to 100 mVs^{-1}). Figure 4 typically shows the cyclic voltammograms recorded in 100 ppm nPANI-HCl suspension at pHs values of − 0.2 and 0.05. With respect to these data, the plot of peak current versus scan rate (I_p vs. ν) for the first anodic peak at different pHs shows a linear behavior (Fig. 5a) indicating that the first oxidation step is likely controlled

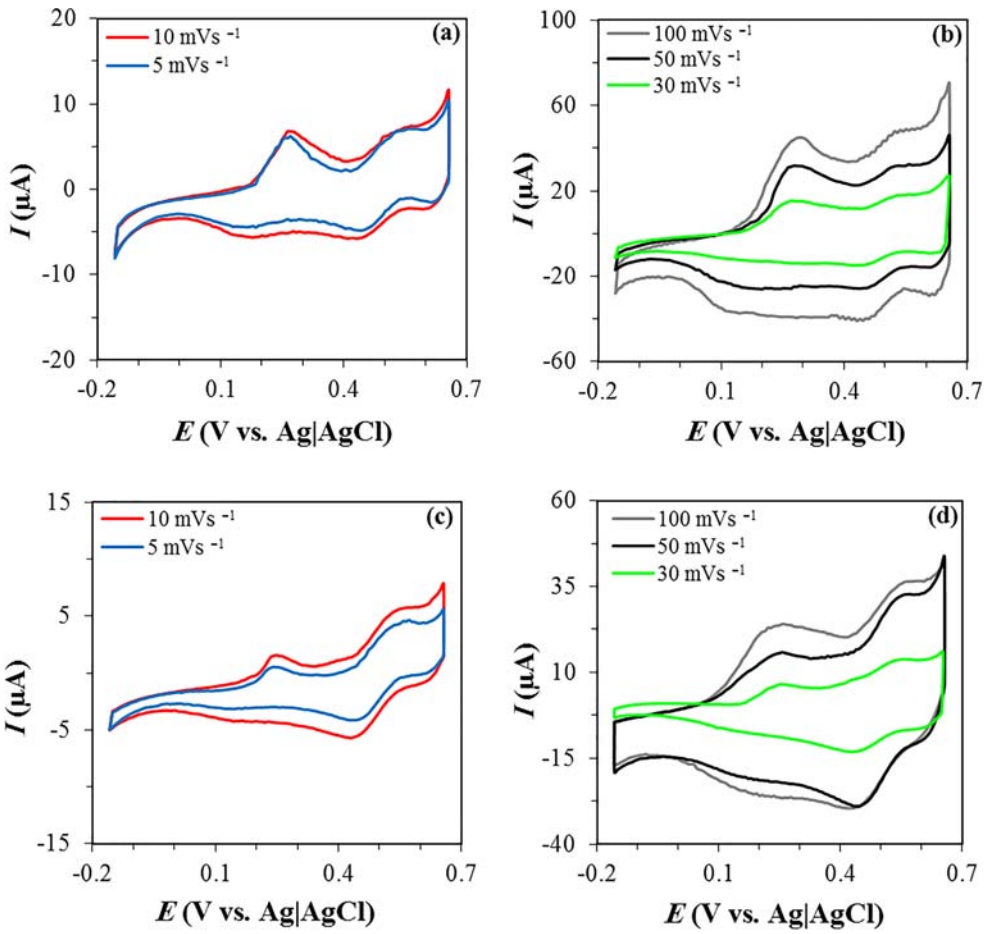

Fig. 4 Cyclic voltammograms recorded for 100 ppm nPANI-HCl suspension at pH − 0.2 and 0.05 at low scan rates: **a** and **c** and high scan rates: **b** and **d**, respectively

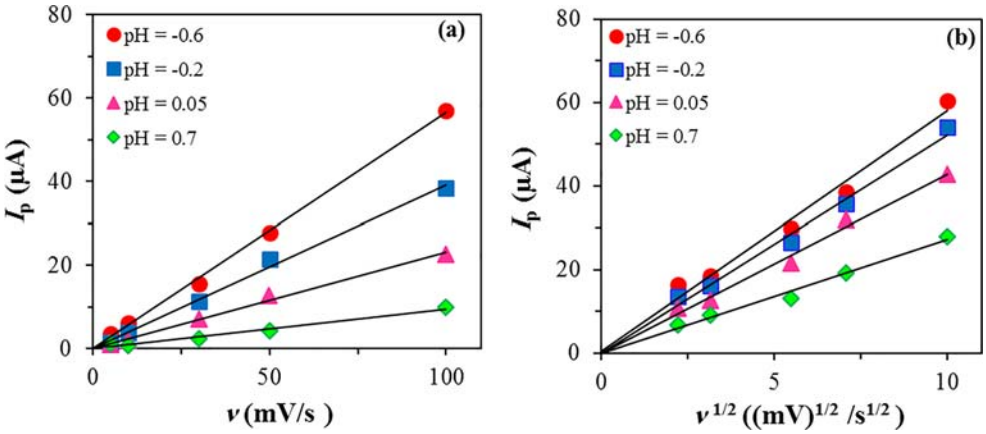

Fig. 5 The plots of peak current vs. scan rate for the first anodic peak (a) and peak current vs. the square root of scan rate for the second anodic peak (b) of 100 ppm nPANI-HCl suspension at different pHs

by the adsorption process where the similar result was reported by the other researchers for a polyaniline film [26, 47]. Furthermore, at a low concentration of polyaniline-coated latex particles, close to that selected in this study, Aoki et al. [39] studied the relation between the peak current and scan rate; they found the adsorption process is the controlling mechanism.

As can be seen from Fig. 4, the charge transfer process of the first peak (LE → ES) for the negative direction of the potential scan is small and ill defined. This behavior may be due to the insufficient time to react during the collision of nanoparticles and the electrode surface, which has been reported previously [30, 39].

In the case of the second anodic peak, Fig. 5b shows that for all pHs, there is a linear dependency between peak current and with $R^2 = 0.99$, indicating that the diffusion controls the second oxidation step (ES → PE) of nPANI particles [48–50]. Note that the relatively large surface area of the electrode supports the hypothesis that the diffusion process is as planar and hence, the influence of radial diffusion is negligible [51]. Moreover, the shift of peak potential to the negative values as a function of scan rate (plot not shown) implies that the charge transfer process of the conversion of ES to PE is an irreversible process. Regarding an irreversible charge transfer associated with a diffusion process, the linear relation between I_p and $\nu^{1/2}$ can be expressed as [52]:

$$I_p = \left(2.99 \times 10^5\right)\left(\alpha\, n'\right)^{1/2} n\, A\, C\, (D\,\nu)^{1/2} \qquad (1)$$

where α is the charge transfer coefficient which is usually assumed to be close to 0.5 [53]. The parameter n' is related to the number of electron transfer for a unit of reaction [54] which is equal to 2 for the PANI structure containing four neighboring aromatic rings. The parameter n corresponds to the number of electrons transferred per nPANI particle diffusing towards the electrode surface [39, 55]. The parameters, A and C, are the electrode surface area and concentration of nPANI particles, respectively. It is worth noting that the diffusion coefficient, D, of nPANI particles ($cm^2\ s^{-1}$) was calculated using the Stokes–Einstein equation [52, 55].

Therefore, parameter n was estimated with respect to Eq. (1) by the slope of the line of plot I_p versus $\nu^{1/2}$ (Fig. 5b). The estimated values for parameters D and n are given in Table 1. The relatively high values (10^4) of parameter n indicate the high electron transfer ability of nPANI suspension. However, the value of n is decreased by increasing the pH of the suspension. This can be explained by the fact that parameter n is also proportional to the number of active sites per nPANI particle; thereby, at the same conditions, the higher acidic suspension provides a greater number of active sites per nPANI particle due to the higher level of protonation.

Chronoamperometry research

The chronoamperometry technique was applied to further study the effect of solution pH on the redox behavior of nPANI-HCl suspension where nPANI particles are initially in the form of ES and they can be transformed to the other forms such as PE or LE near the electrode surface under applying a one-step potential. However, in the case of polyaniline film, researchers have been applied two transformation steps including a full oxidation step followed by the reduction process [56, 57].

Figure 6 shows the effect of solution pH on the chronoamperometry curves of nPANI particles at different concentrations varying between 0 and 100 ppm in HCl solution. For these experiments, the reduction potential was individually chosen for each solution pH with respect to the CV

Table 1 The effect of solution pH on the diffusion parameters of 100 ppm nPANI-HCl suspension

pH	− 0.60	− 0.20	0.05	0.70
D ($cm^2\ s^{-1}$)	7.92×10^{-8}	9.01×10^{-8}	9.14×10^{-8}	9.50×10^{-8}
n	3.83×10^4	3.24×10^4	2.64×10^4	1.64×10^4

curves (Fig. 2) where the transformation between ES and LE occurs. With respect to this concept, the negative sign of current satisfies the fact that the reduction and de-doping of ES to LE occurs. Figure 6 shows that for all systems, current decreases quickly at the early period of measurement and then reaches a steady value known as the residual current. When the quantity of nPANI particles increases, the residual current decreases which can be related to the higher coverage of electrode with a nonconductive layer of LE causing a decrease in the reduction rate of nPANI particles [31].

On the other hand, it can be found from Fig. 6 that at a constant concentration of nPANI particles, e.g., 100 ppm, when pH increases from − 0.60 to 0.70, the value of residual current increases from 0.55 to 1.23 μA in the cathodic direction. This can be explained by the fact that the higher acidic condition provides a higher protonation level of amine and imine groups [29, 58].

The adsorption behavior of nPANI particles at the electrode surface was studied with the adsorption isotherms. The experimental data showed a linear relation of C/θ versus C, indicating that the adsorption obeys the Langmuir isotherm that is given by the following equation [59, 60]:

$$\frac{C}{\theta} = \frac{1}{K_{ads}\,\theta_{max}} + \frac{C}{\theta_{max}} \tag{2}$$

where K_{ads} is the adsorption constant ($cm^3\ mol^{-1}$), θ is the fraction of the surface coverage and θ_{max} is the maximum fraction of the surface coverage by a monolayer of nPANI particles. The value of θ can be calculated using the following equation:

$$\theta = \frac{I_0 - I}{I_0} \tag{3}$$

where I_0 and I are the residual current in the absence and presence of nPANI particles, respectively. The experimental data were well fitted to Eq. (2) and the linear plot of C/θ versus C is shown in inset Fig. 6. Therefore, the isotherm constants including θ_{max} and K_{ads} were calculated from the slope and intercept of the plots, respectively. K_{ads} can be related to the free adsorption energy (ΔG^0_{ads}, J mol^{-1}) by using the following equation [60]:

$$K_{ads} = \frac{1}{55.5}\exp\left(-\frac{\Delta G^0_{ads}}{RT}\right) \tag{4}$$

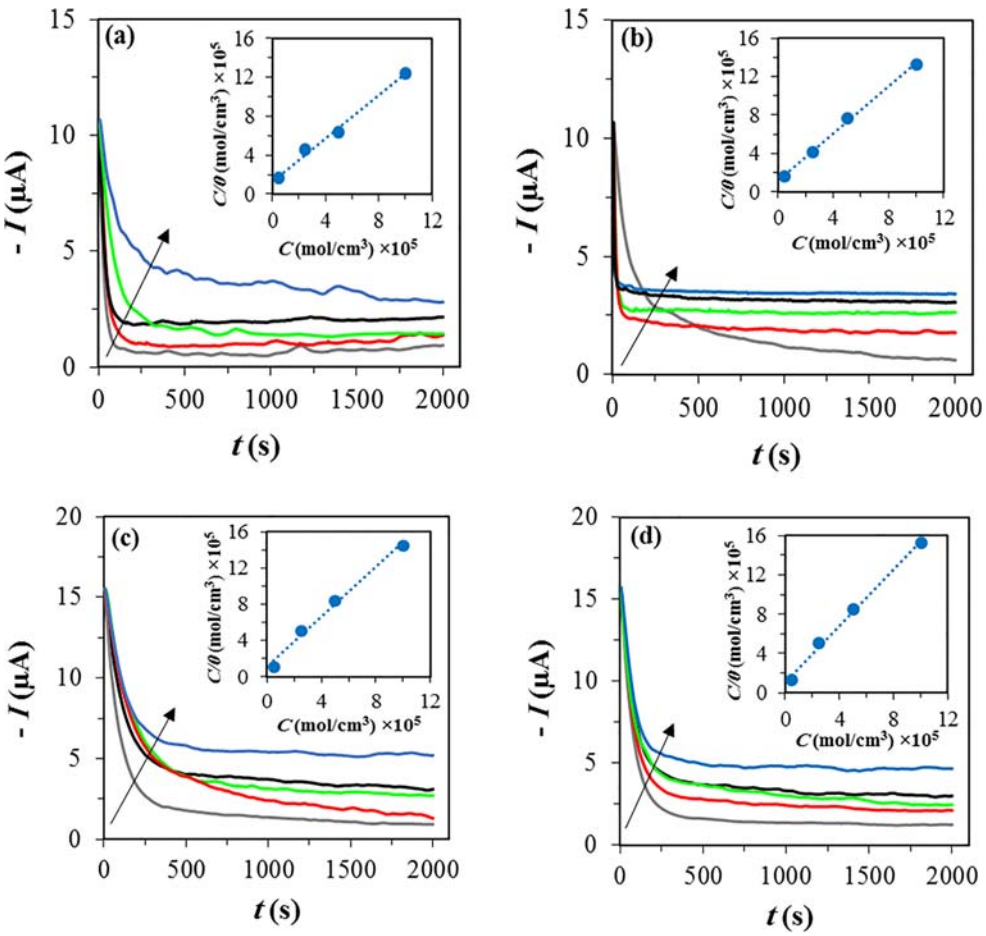

Fig. 6 Effect of nPANI particle concentration on the chronoamperograms of nPANI particles at different concentrations; blank 100 (gray), 50 (red), 25 (yellow-green), 5 (black), and 0 (blue) ppm; in HCl solution and at different pH values: **a** − 0.60, **b**− 0.20, **c** 0.05, and **d** 0.70. Inset: Langmuir isotherm for nPANI-HCl suspensions

where R is the universal gas constant and T is the absolute temperature (here T = 298 K). The values of adsorption parameters, θ_{max}, K_{ads}, and ΔG^0_{ads} are given in Table 2. The negative sign of ΔG^0_{ads} at all pHs approves that the adsorption process of nPANI particles at the electrode surface occurs spontaneously. In addition, the values of ΔG^0_{ads} are around − 20 kJ mol^{-1} confirming the physisorption of nPANI particles in all suspensions [61].

According to Table 2, at the higher acidic condition, the maximum fraction of surface coverage (θ_{max} (increases, reflecting the higher adsorption capacity of nPANI particles on the electrode surface. Furthermore, at the same time, ΔG^0_{ads} shifts slightly to more negative values, suggesting the stronger adsorption of nPANI particles with the increment of pH.

This behavior can be explained by the co-operative effect [62, 63], besides the direct adsorption of nPANI particles, where protonated nPANI particles can be electrostatically adsorbed onto the halide-covered electrode surface through the hydrogen atom. In this situation, the higher protonation state of nPANI particles favors higher surface coverage but may reduce the establishment of adsorption towards the electrode surface.

The nPANI particles are adsorbed on the electrode surface in two ways: either adsorbed directly on the surface or the protonated nPANI are adsorbed onto the halide-covered electrode surface through the hydrogen atom, which is called the co-operative effect. Therefore, the higher protonation state of nPANI particles (which is obtained under more acidic conditions and lower pH) approves the more adsorption and the higher the coverage on the electrode surface. On the other hand, the co-operative effect likely reduces the stable and direct adsorption on the electrode surface, so the adsorption strength is slightly stronger as the pH of the suspension increases.

The effect of solution pH at different concentrations of nPANI particle and at the potential 0.65 V vs. Ag|AgCl on the second oxidation peak, controlled by the diffusion process, was further studied using the chronoamperometry method and the registered data are presented in Fig. 7. The intensive decrease in the oxidation current at the early time has likely arisen from rapidly consumption of ES particles adjacent to the electrode surface by the conversion to PE form. Moreover, the residual current increases with the nPANI particle concentration. These observations demonstrate that the diffusion of nPANI particles controls the oxidation process.

In these conditions, the chronoamperometry data, obtained for the electrochemical conversion of nPANI particles (ES → PE), was quantitatively analyzed using Cottrell's law [64, 65]:

$$I = \frac{n\ \mathrm{F}\ A\ C\ D^{1/2}}{\pi^{1/2}\ t^{1/2}} \tag{5}$$

where F is the Faraday constant. The linear plots of I vs. $t^{-1/2}$ for the suspensions with a concentration of 100 ppm nPANI particles and at different pH values are displayed in the inset of Fig. 7. The slope of this straight line is commonly used to estimate the value of the diffusion coefficient of dopants for a PANI film [57, 66]. However, here, the diffusion process is attributed to the nPANI particles within the solution and hence, the value of D was estimated by the Stokes–Einstein equation [39, 55]. Therefore, the values of parameter n (the number of electrons transferred per nPANI particle) at different pHs were estimated and are presented in Table 3. The increase of pH is associated with the decrease of parameter n where this trend of variation is consistent with the CV results (Table 1) and has been discussed in the previous section. However, the values of parameter n, obtained by the chronoamperometry test, is higher compared to that for CV test. It is probably arisen from the fact that in the chronoamperometry test, the nPANI particles have a higher time for the electron transfer process.

The high value of parameter n suggests the advantage of this system in the improvement of diverse practical plans such as anti-corrosion agents, ion exchange, and supercapacitors based on the redox properties of polyaniline where the nPANI particles are as a disperse phase in an electrolyte solution and they could be adsorbed onto the electrode surface to improve the electrochemical properties.

Table 2 Effect of solution pH on the adsorption parameters calculated from the chronoamperometry data for nPANI-HCl suspension at T = 298 K

pH	θ_{max}	K_{ads} (m^3 mol^{-1})	− ΔG_{ads} (kJ mol^{-1})
− 0.60	0.90	110.3	21.6
− 0.20	0.81	122.1	21.9
0.05	0.73	137.5	22.2
0.70	0.69	143.9	22.3

Evaluation of nPANI adsorption by FE-SEM/EDX

At the end of the chronoamperometry test under E = 0.65 V vs. Ag|AgCl at pH − 0.60 and 0.70, the electrode surface was inspected using FE-SEM images and EDX analysis and the results are shown in Fig. 8. For both suspensions, the existence of spherical shaped nPANI particles on the electrode surface satisfies the adsorption of nPANI particles. However, the accumulation of nPANI particles on the electrode surface is likely related to the continued adsorption of these particles not to a precipitation phenomenon because of the uniform dispersion of nPANI particles and the suspension stability during the time. The existence of intensive peak for carbon element, detected by elemental analysis with EDX, approves

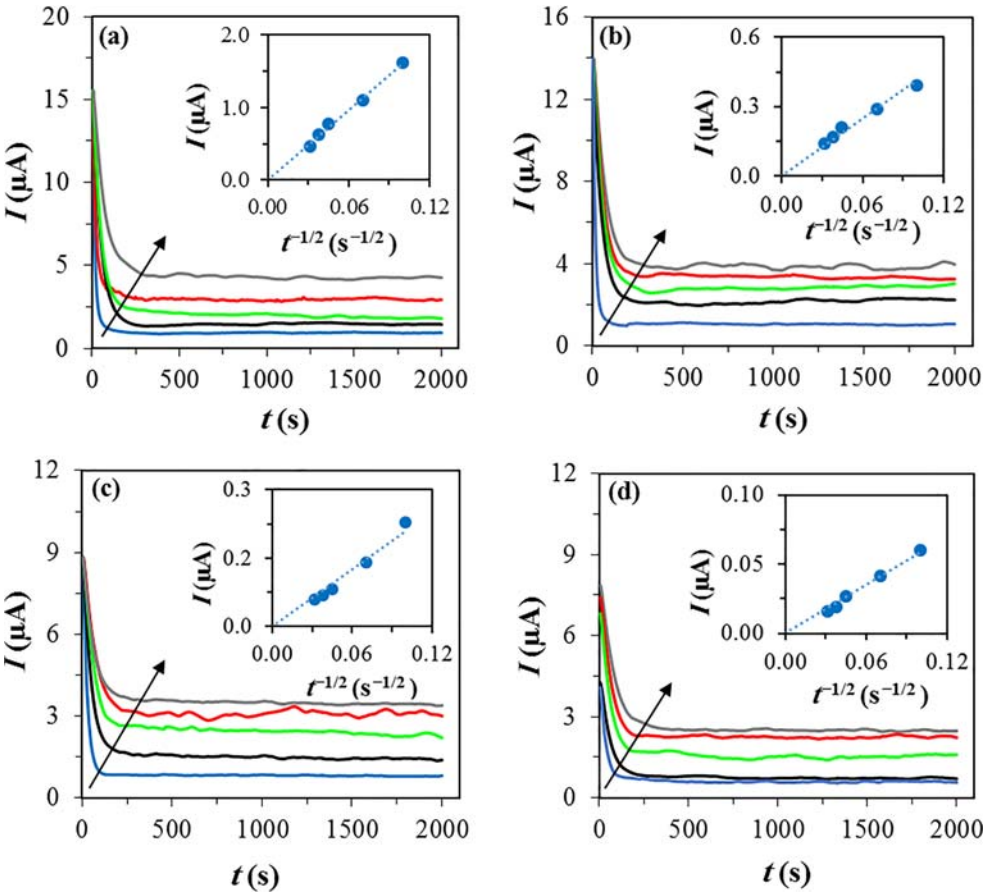

Fig. 7 Effect of nPANI particle concentration (blank 100 (gray), 50 (red), 25 (yellow-green), 5 (black), and 0 (blue) ppm) on the chronoamperograms of nPANI particle suspension and at different pH values: **a** − 0.60, **b** − 0.20, **c** 0.05 and **d** 0.70. Inset: the plot of I vs. $t^{-1/2}$ for the suspensions at a concentration of 100 ppm nPANI particles

additionally nPANI particles could adsorb on the electrode surface.

The effect of solution pH on the adsorption was qualitatively evaluated using microstructural image processing (MIP) according to the procedure proposed by ASTM E562 (figures not shown). This analysis showed that the phase fraction of nPANI particles, adsorbed on the electrode, at pH = − 0.60 is higher than that for pH = 0.70, which is in good agreement with the chronoamperometry results (see Table 2).

DFT calculation and MC simulation

The effect of pH at values of 0.70 and − 0.60 on the adsorption of nPANI particles was theoretically evaluated using computational calculations. To this end, two different structures of partly (PANI-I) and completely (PANI-II) protonated PANI, corresponding to pH 0.70 and − 0.60, respectively, were defined to quantum chemical study and MC simulation. The geometry of emeraldine form for both of these structures was as the closed-shell phenyl-capping tetramer because its angles and bond distances had a good agreement with the actual structure of polyaniline [67].

Table 3 The effect of solution pH on the total number of active sites per nPANI particle, n, at 100 ppm concentration

pH	− 0.60	− 0.20	0.05	0.70
n	5.70×10^6	1.42×10^6	7.12×10^5	1.1×10^5

The optimized molecular structures, HOMO and LUMO orbitals for PANI-I and PANI-II molecules, are shown in Figs. 9 and 10, respectively. The HOMO and LUMO are the highest occupied and lowest unoccupied molecular orbital where can donate an electron and accept an electron, respectively [68]. The electron density distribution of HOMO for PANI-I (Fig. 9b) demonstrates that the aromatic rings on the right side have a larger electric density. It is suggested that the aromatic rings are the most probable sites for donating an electron to vacant orbitals of the Au surface, while LUMO distribution is mainly focused in the middle of the molecule.

For the optimized structure of PANI-II, displayed in Fig. 10, both HOMO and LUMO are equally localized on the aromatic rings at both sides of the polyaniline molecule, suggesting a parallel adsorption of PANI-II molecules onto the Au surface. Thus, it is sensible to assume that PANI-II includes more adsorption centers, leading likely to the higher adsorption ability than PANI-I.

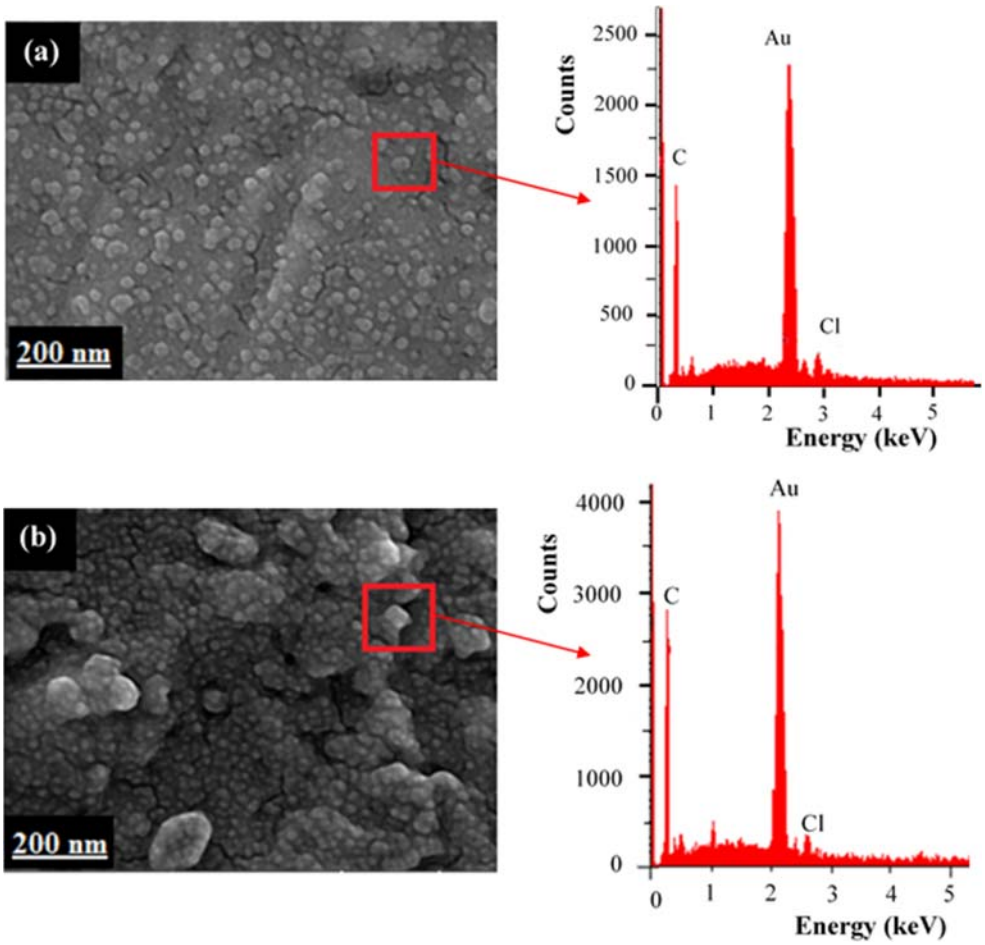

Fig. 8 FE-SEM micrographs of the gold electrode surface in nPANI-HCl suspension at the pH **a** − 0.60 and **b** 0.70. The arrows indicate the adsorbed nPANI particles, identified by EDX analysis

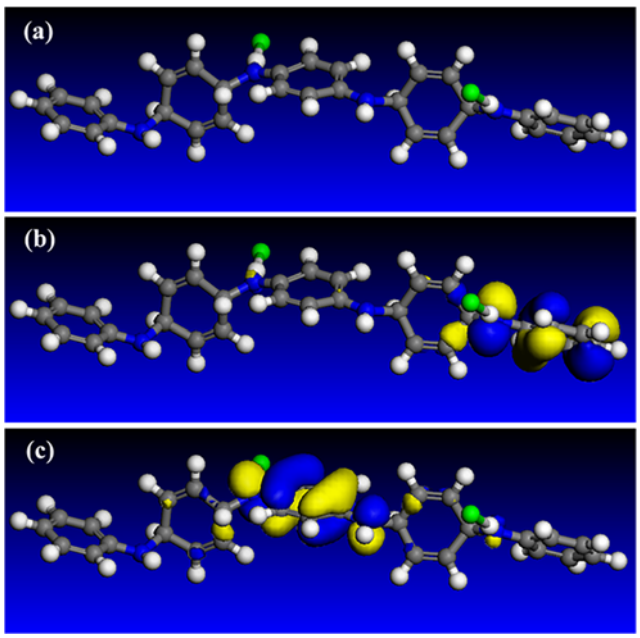

Fig. 9 Optimized structures (a), HOMO (b), and LUMO (c) of PANI-I, corresponding to pH 0.70, obtained by DFT using the DMol^3 method

The quantum chemical parameters including E_{HOMO}, E_{LUMO}, energy gap ($\Delta E = E_{LUMO} - E_{HOMO}$), and dipole moment ($\mu$) for the PANI-I and PANI-II molecules are presented in Table 4.

It can be found that PANI-I has a higher value of E_{HOMO} than that for PANI-II. It can be deduced that PANI-I has a higher capability to donate electrons to the vacant d-orbital of Au atoms. While the low value of E_{LUMO} for PANI-II advices the higher ability of electron accepting in comparison with PAIN-I. These behaviors can be related to the protonation level of the polyaniline chain. Since the structure of PANI-I is partly protonated and doped, another nitrogen tends to donate electrons, but in the structure of PANI-II, all nitrogen atoms are completely protonated and have high tendency to accept electrons.

According to the data presented in Table 4, PANI-II has a lower value of ΔE than that for PANI-I, indicating the complete protonation structure of PANI has a higher tendency to adsorb onto the gold surface. Furthermore, the value of μ for PANI-II is lower than that for PANI-I. Some researchers reported that the low value of dipole moment is an indication of the accumulation of organic molecules at the metal surface by

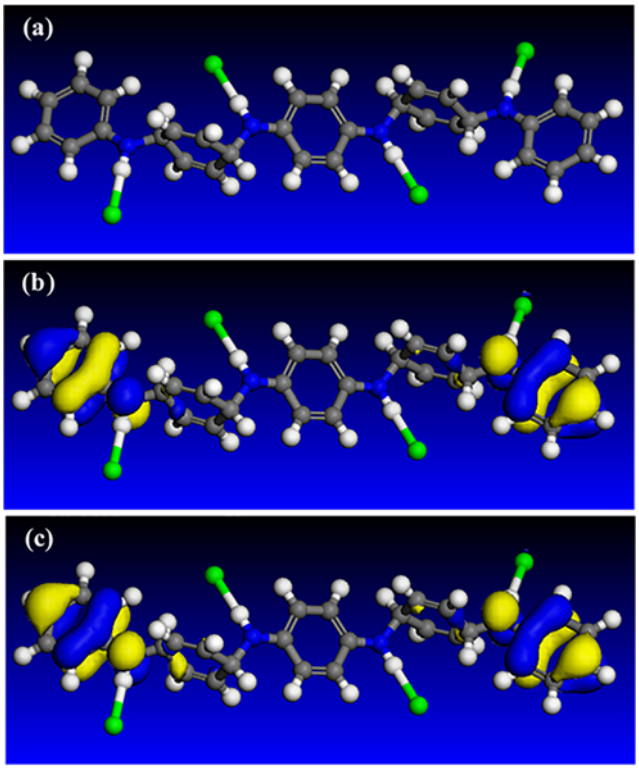

Fig. 10 Optimized structures (**a**), HOMO (**b**), and LUMO (**c**) of PANI-II, corresponding to pH − 0.60, obtained by DFT using the DMol^3 method

this means increasing the inhibition ability [69, 70]. In the present work, the higher surface coverage for PANI-II, obtained by electrochemical methods, can be explained by the lower value of dipole moment.

To further study the effect solution pH on the adsorption behavior of PANI in HCl solution, MC simulations were performed in the presence of water and HCl molecules on Au (110) plane surface; thus, the adsorption configuration of a single PANI-I and PANI-II molecule in the presence of HCl and H_2O molecules are displayed in Figs. 11 and 12, respectively. The side view of the most stable adsorption configurations shows that PANI-I and PANI-II are adsorbed from one side and both sides, respectively as a result of the difference in the position of both the HOMO and LUMO sites. This suggests that the adsorption direction of polyaniline depends on the solution pH.

The total energy (the sum of adsorption energy and the internal energy of the adsorbate), adsorption energy, and the

Table 4 The parameters of quantum chemical calculations for the PANI-I and PANI-II molecules

Sample	E_{HOMO} (eV)	E_{LUMO} (eV)	ΔE (eV)	μ (Debye)
PANI-I	− 5.1	− 3.4	1.7	1.30
PANI-II	− 5.8	− 4.2	1.6	0.05

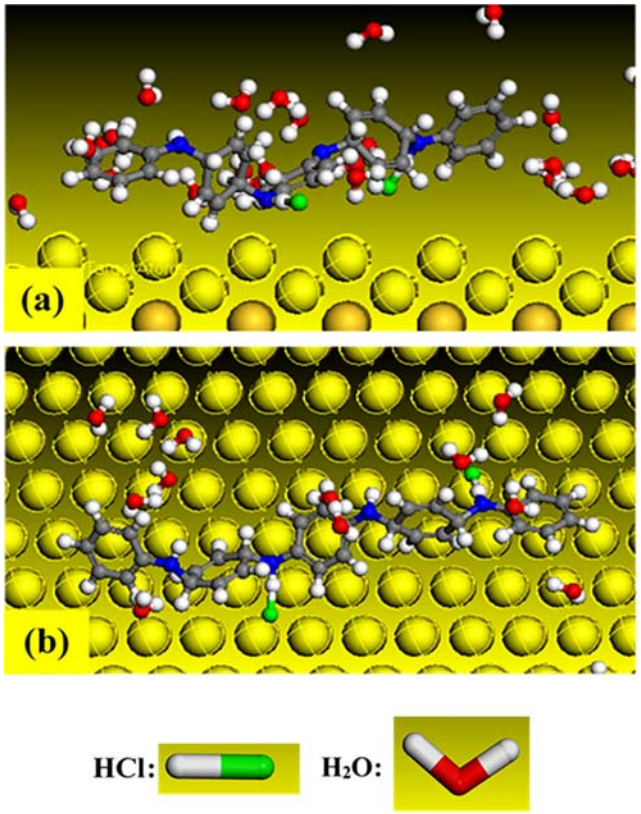

Fig. 11 The side (**a**) and top (**b**) view of the most stable configuration for the adsorption of PANI-I (related to pH 0.70) on Au (110) plane surface, obtained using Monte Carlo simulations

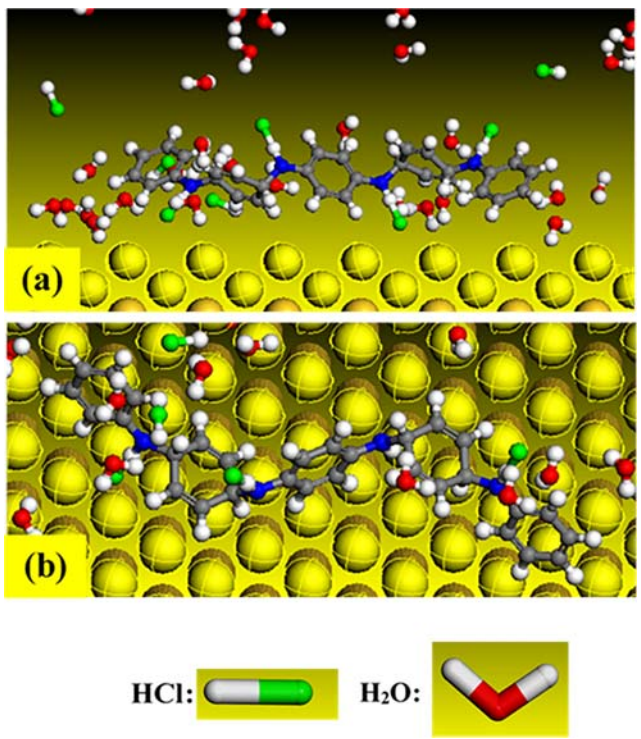

Fig. 12 The side (**a**) and top (**b**) view of the most stable configuration for the adsorption of PANI-II (related to pH − 0.60) on Au (110) plane surface obtained using Monte Carlo simulations

Table 5 Outputs obtained from the MC simulation for adsorption of two structures of PANI molecule on Au (110) (in kJ mol^{-1})

Sample	Total energy	Adsorption energy	H_2O: dE_{ad}/dN_i	HCl: dE_{ad}/dN_i	PANI-HCl: dE_{ad}/dN_i
PANI-I	-11×10^4	-9.5×10^4	0.5	0.7	− 101
PANI-II	-10×10^4	-8.0×10^4	3.0	0.5	− 52

differential adsorption energy (dE_{ad}/dN_i) calculated by MC simulations are given in Table 5. Accordingly, the higher adsorption and total energy of the PANI-I molecule compared to the PANI-II molecule demonstrate the higher stability of adsorption configuration at pH 0.70 [71]. Therefore, both the quantum chemical calculations and MC simulations explain the reason for the higher value of ΔG_{ads} for PANI-I obtained from electrochemical data (Table 2).

From Table 5, the lower absolute value of dE_{ad}/dN_i for H_2O and HCl compared with that for the PANI-HCl molecule suggests that they can be easily substituted by polyaniline molecules [69]. This behavior is due to the higher affinity of polyaniline molecules to adsorb on the Au surface, which is in good agreement with the values of free adsorption energies (in Table 2).

Conclusions

The effect of solution pH, varying in the strong acidic region, on the electrochemical response of a stable nPANI particle suspension was carefully investigated by different electrochemical and surface analysis methods. The main results are listed as follows:

i. Cyclic voltammetry measurements demonstrated that the charge transfer process for the conversion between LE and ES form (first oxidation peak) is controlled by the adsorption nPANI particle. At the higher potentials, a redox couple specified the transformation of ES to a fully oxidized form of polyaniline (PE) controls through the diffusion mechanism of nPANI particles. Furthermore, the controlling mechanisms were satisfied by the chronoamperometry results.
ii. The electrochemical results showed that for the first oxidation peak, the peak potential decreases with solution pH by a linear relation where the slope of 60 mV per pH unit indicating a complete protonation process while for pH > 0.05, the intensity of variations decreases significantly suggesting the partly protonation of nPANI structure. However, at more acidic condition, the peak current values increase through the enhancement of protonation level of nPANI.
iii. The quantitative analysis of electrochemical results showed that the decrease of pH causes the higher and stronger adsorption of nPANI particles on the gold electrode. Moreover, the number of electrons (parameter n) transferred per nPANI particle which diffused near the electrode surface increases at the higher acidic condition. The high value of this parameter indicates that nPANI particles could efficiently participate in redox reactions.
iv. The effect of pH on the adsorption phenomenon of nPANI particle at the electrode surface was confirmed by both surface analysis methods (FE-SEM images and EDX analysis) and theoretical studies carried out by quantum and MC simulations.
v. Theoretical investigation demonstrated that in the more acidic conditions, the lower value of dipole moment and the existence of HOMO and LUMO orbitals at both sides of nPANI particles describe the higher surface coverage of electrode. However, the adsorption is slightly stronger and stable for the higher pH values as a result of the higher adsorption energy. These are in good agreement with those obtained by the electrochemical methods.
vi. In the present work, nanoparticles of polyaniline (nPANI particle) have unique characteristics, including excellent electrochemical behavior and good absorption on the surface of the electrode, making it a promising material for improving the performance of anti-corrosion agent, ion exchange process, and PANI-based supercapacitors.

Acknowledgment We highly appreciate Khorasan Razavi Gas Co. for their provision of laboratory facilities for conducting the experiments required in this research study. And, we hereby acknowledge that part of this computation was performed on the HPC center of the Ferdowsi University of Mashhad.

References

1. Bhadra S, Khastgir D, Singha NK, Lee JH (2009) Progress in preparation, processing and applications of polyaniline. Prog Polym Sci 34(8):783–810
2. Boeva ZA, Sergeyev VG (2014) Polyaniline: synthesis, properties, and application. Polym Sci Ser C 56(1):144–153
3. Marjanović GĆ (2013) Recent advances in polyaniline research: polymerization mechanisms, structural aspects, properties and applications. Synth Met 177:1–47
4. Soni A, Pandey CM, Pandey MK, Sumana G (2019) Highly efficient polyaniline-MoS_2 hybrid nanostructures based biosensor for cancer biomarker detection. Anal Chim Acta 1055:26–35
5. Singh S, Solanki PR, Pandey MK, Malhotra BD (2006) Covalent immobilization of cholesterol esterase and cholesterol oxidase on polyaniline films for application to cholesterol biosensor. Anal Chim Acta 568(1-2):126–132

6. Ardakani MM, Mohseni MAS, Alibeik MA (2013) Fabrication of an electrochemical sensor based on nanostructured polyaniline doped with tungstophosphoric acid for simultaneous determination of low concentrations of norepinephrine, acetaminophen and folic acid. J Mol Liq 178:63–69
7. Jain R, Tiwari DC, Karolia P (2014) Electrocatalytic detection and quantification of Nitazoxanide based on graphene- polyaniline (Grp-Pani) nanocomposite sensor. J Electrochem Soc 161(12): H839–H844
8. Xu H, Zhang J, Chen Y, Lu H, Zhuang J (2014) Electrochemical polymerization of polyaniline doped with Zn^{2+} as the electrode material for electrochemical supercapacitors. J Solid State Electrochem 18(3):813–819
9. Asen P, Shahrokhian S, Zad AI (2018) Transition metal ions-doped polyaniline/graphene oxide nanostructure as high performance electrode for supercapacitor applications. J Solid State Electrochem 22(4):983–996
10. Wang H, Ma L, Gan M, Zhou T, Sun X, Dai W, Wang H, Wang S (2016) Synthesis of polyaniline/HF partially etched-hierarchical porous TiO_2 microspheres composite with high electrochemical performance for supercapacitors. J Solid State Electrochem 20(2):525–532
11. Ghanbari K, Mousavi MF, Shamsipur M (2006) Preparation of polyaniline nanofibers and their use as a cathode of aqueous rechargeable batteries. Electrochim Acta 52(4):1514–1522
12. Wang Z, Han J, Zhang N, Sun D, Han T (2019) Synthesis of polyaniline/graphene composite and its application in zinc-rechargeable batteries. J Solid State Electrochem 23(12):3373–3382
13. Tallman DE, Spinks G, Dominis A, Wallace GG (2002) Electroactive conducting polymers for corrosion control Part 1. General introduction and a review of non-ferrous metals. J Solid State Electrochem 6(2):73–84
14. Kosseoglou D, Kokkinofta R, Sazou D (2011) FTIR spectroscopic characterization of Nafion®–polyaniline composite films employed for the corrosion control of stainless steel. J Solid State Electrochem 15(11-12):2619–2631
15. Yano J, Muta A, Harima Y, Kitani A (2011) Poly(2,5-dimethoxyaniline) film coating for corrosion protection of iron. J Solid State Electrochem 15(3):601–605
16. Chen J, Hong X, Zhao Y, Xia Y, Li D, Zhang Q (2013) Preparation of flake-like polyaniline/montmorillonite nanocomposites and their application for removal of Cr(VI) ions in aqueous solution. J Mater Sci 48(21):7708–7717
17. Javadian H, Ghaemy M, Taghavi M (2014) Adsorption kinetics, isotherm, and thermodynamics of Hg^{2+} to polyaniline/hexagonal mesoporous silica nanocomposite in water/wastewater. J Mater Sci 49(1):232–242
18. Chiang JC, MacDiarmid AG (1986) Polyaniline: protonic acid doping of the emeraldine form to the metallic regime. Synth Met 13(1-3):193–205
19. MacDiarmid AG, Epstein AJ (1989) Polyanilines: a novel class of conducting polymers. Faraday Discuss Chem Soc 88:317–332
20. Huang WS, Humphrey BD, MacDiarmid AG (1986) Polyaniline, a novel conducting polymer. Morphology and chemistry of its oxidation and reduction in aqueous electrolytes. J Chem Soc Farad T 1(82):2385–2400
21. Trivedi D (1998) Influence of the anion on polyaniline. J Solid State Electrochem 2(2):85–87
22. Ray A, Richter AF, MacDiarmid AG (1989) Polyaniline: protonation/deprotonation of amine and imine sites. Synth Met 29:l51–l56
23. Scotto J, Florit MI, Posadas D (2018) Redox commuting properties of polyaniline in hydrochloric, sulphuric and perchloric acid solutions. J Electroanal Chem 817:160–166
24. Kalaji M, Nyholm L, Peter LM (1991) A microelectrode study of the influence of pH and solution composition on the electrochemical behaviour of polyaniline films. J Electroanal Chem 313(1-2): 271–289
25. Yan R, Jin B, Li D, Qian C, Tan X (2017) Temperature dependence of hydrogen bond in the redox process of polyaniline. J Electrochem Soc 164(7):H521–H525
26. Gao M, Yang Y, Diao M, Wang S, Wang X, Zhang G, Zhang G (2011) Exceptional ion-exchange selectivity for perchlorate based on polyaniline films. Electrochim Acta 56(22):7644–7650
27. Hao Q, Lei W, Xia X, Yan Z, Yang X, Lu L, Wang X (2010) Exchange of counter anions in electropolymerized polyaniline films. Electrochim Acta 55(3):632–640
28. Scotto J, Flori MI, Posadas D (2016) pH dependence of the voltammetric response of Polyaniline. J Electroanal Chem 785: 14–19
29. Ping Z, Nauer GE, Neugebauer H, Theiner J, Neckel A (1997) Protonation and electrochemical redox doping processes of polyaniline in aqueous solutions: investigations using in situ FTIR-ATR spectroscopy and a new doping system. J Chem Soc Farad T 1(93):121–129
30. Nazari H, Arefinia R (2019) Electrochemical and quantum chemical study of polyaniline nanoparticles suspension in HCl and H_2SO_4. Electrochim Acta 320:134553
31. Nazari H, Arefinia R (2019) Electrochemical behavior of polyaniline nanoparticles suspension: adsorption and diffusion. J Mol Liq 288:110999
32. Nazari H, Arefinia R (2019) An investigation into the relationship between the electrical conductivity and particle size of polyaniline in nano scale. Int J Polym Anal Ch 24(2):178–190
33. David TMS, Arasho W, Smith O, Hong K, Bonner C, Sun SS (2017) Self-assembly and charge transport of a conjugated polymer on ITO substrates. Polym Sci 3:1–8
34. Bard AJ, Faulkner LR (2001) Electrochemical methods fundamentals and applications. John Wiley & Sons, New York
35. Arefinia R, Shojaei A, Shariatpanahi H, Neshati J (2012) Anticorrosion properties of smart coating based on polyaniline nanoparticles/epoxy-ester system. Prog Org Coat 75(4):502–508
36. Hunter RJ (1981) Zeta potential in colloid science. Academic Press, New York
37. Wan M (1992) Absorption spectra of thin film of polyanilin. J Polym Sci A Polym Chem 30(4):543–549
38. Stejskal J, Kratochvíl P, Radhakrishnan N (1993) Polyaniline dispersions 2. UV—Vis absorption spectra. Synth Met 61(3):225–231
39. Aoki K, Chen J, Ke Q, Armes SP, Randall DP (2003) Redox reactions of polyaniline-coated latex suspensions. Langmuir 19(13): 5511–5516
40. Park HW, Kim T, Huh J, Kang M, Lee JE, Yoon H (2012) Anisotropic growth control of polyaniline nanostructures and their morphology-dependent electrochemical characteristics. ACS Nano 6(9):7624–7633
41. Pruneanu S, Veress E, Marian I, Oniciu L (1999) Characterization of polyaniline by cyclic voltammetry and UV-Vis absorption spectroscopy. J Mater Sci 34(11):2733–2739
42. Liu J, Zhu G, Li X, McAuley CB, Sokolov SV, Compton RG (2017) Quantifying charge transfer to nanostructures: polyaniline nanotubes. Appl Mater Today 7:239–245
43. Lei T, Aoki K (2000) Monodispersed redox submicrometer particles created by polyaniline-coated polystyrene latex. J Electroanal Chem 482(2):149–155
44. Wopschall RH, Shain I (1967) Effects of adsorption of electroactive species in stationary electrode polarography. Anal Chem 39(13): 1514–1527
45. Marmisollé WA, Florit MI, Posadas D (2013) Coupling between proton binding and redox potential in electrochemically active

macromolecules. The example of Polyaniline. J Electroanal Chem 707:43–51
46. Marmisolle´ WA, Florit MI, Posadas D (2010) The coupling among electron transfer, deformation, screening and binding in electrochemically active macromolecules. Phys Chem Chem Phys 12(27):7536–7544
47. Pauliukaite R, Brett CMA, Monkman AP (2004) Polyaniline fibres as electrodes. Electrochemical characterisation in acid solutions. Electrochim Acta 50:159–167
48. Dlugosz AP, Socha A, Rynkowski J (2017) Electrochemical reactions of sodium 2-ethylhexyl sulfate salt. Electrocatalysis 8(3):270–278
49. Ni JA, Ju HX, Chen HY, Leech D (1999) Amperometric determination of epinephrine with an osmium complex and nafion double-layer membrane modified electrode. Anal Chim Acta 378(1-3): 151–157
50. Santos DMF, Sequeira CAC (2010) Cyclic voltammetry investigation of borohydride oxidation at a gold electrode. Electrochim Acta 55(22):6775–6781
51. Ngamchuea K, Eloul S, Tschulik K, Compton RG (2014) Planar diffusion to macro disc electrodes—what electrode size is required for the Cottrell and Randles-Sevcik equations to apply quantitatively? J Solid State Electrochem 18(12):3251–3258
52. Brownson DAC, Banks CE (2014) The handbook of graphene electrochemistry. Springer, London
53. Eklund JC, Bond AM, Alden JA, Compton RG (1999) Perspectives in modern voltammetry: basic concepts and mechanistic analysis. Adv Phys Org Chem 32:1–120
54. Aoki K, Lei T (2000) Electrochemical event of single redox latex particles. Langmuir 16(26):10069–10075
55. Beasley CA, Murray RW (2009) Voltammetry and redox charge storage capacity of ferrocene-functionalized silica nanoparticles. Langmuir 25(17):10370–10375
56. Inzelt G (2000) Simultaneous chronoamperometric and quartz crystal microbalance studies of redox transformations of polyaniline films. Electrochim Acta 45(22-23):3865–3876
57. Zhang L, Dong S (2004) The electrocatalytic oxidation of ascorbic acid on polyaniline film synthesized in the presence of camphorsulfonic acid. J Electroanal Chem 568:189–194
58. Ybarra G, Moina C, Florit MI, Posadas D (2000) Proton exchange during the redox switching of polyaniline film electrodes. Electrochem Solid-State Lett 3:330–332
59. Farcas M, Cosman NP, Ting DK, Roscoe SG, Omanovic S (2010) A comparative study of electrochemical techniques in investigating the adsorption behaviour of fibrinogen on platinum. J Electroanal Chem 649(1-2):206–218
60. Jackson DR, Omanovic S, Roscoe SG (2000) Electrochemical studies of the adsorption behavior of serum proteins on titanium. Langmuir 16(12):5449–5457
61. Heydari H, Talebian M, Salarvand Z, Raeissi K, Bagheri M, Golozar MA (2018) Comparison of two Schiff bases containing O-methyl and nitro substitutes for corrosion inhibiting of mild steel in 1 M HCl solution. J Mol Liq 254:177–187
62. Haddad MNE (2016) Inhibitive action and adsorption behavior of cefotaxime drug at copper/hydrochloric acid interface: electrochemical, surface and quantum chemical studies. RSC Adv 6(63): 57844–57853
63. Jeyaprabha C, Sathiyanarayanan S, Venkatachari G (2005) Co-adsorption effect of polyaniline and halide ions on the corrosion of iron in 0.5 M H_2SO_4 solutions. J Electroanal Chem 583(2):232–240
64. Aoki K, Baars A, Jaworski A, Osteryoung J (1999) Chronoamperometry of strong acids without supporting electrolyte. J Electroanal Chem 472(1):1–6
65. Denuault G, Mirkin MV, Bard AJ (1991) Direct determination of diffusion coefficients by chronoamperometry at microdisk electrodes. J Electroanal Chem 308(1-2):27–38
66. Levi M, Markevich E, Aurbach D (2005) Comparison between Cottrell diffusion and moving boundary models for determination of the chemical diffusion coefficients in ion-insertion electrodes. Electrochim Acta 51(1):98–110
67. Kwon O, McKee ML (2000) Calculations of band gaps in polyaniline from theoretical studies of oligomers. J Phys Chem B 104(8):1686–1694
68. Gece G (2008) The use of quantum chemical methods in corrosion inhibitor studies. Corros Sci 50(11):2981–2992
69. Qiang Y, Guo L, Zhang S, Li W, Yu S, Tan J (2016) Synergistic effect of tartaric acid with 2, 6-diaminopyridine on the corrosion inhibition of mild steel in 0.5 M HCl. Sci Rep 6(1):33305
70. Guo L, Zhu S, Zhang S, He Q, Li W (2014) Theoretical studies of three triazole derivatives as corrosion inhibitors for mild steel in acidic medium. Corros Sci 87:366–375
71. Khaled KF (2009) Monte Carlo simulations of corrosion inhibition of mild steel in 0.5 M sulphuric acid by some green corrosion inhibitors. J Solid State Electrochem 13(11):1743–1756